New look at the degeneracies in the neutrino oscillation parameters, and their resolution by T2K, NOνA and ICAL

Monojit Ghosh,[1,*] Pomita Ghoshal,[2,†] Srubabati Goswami,[1,‡] Newton Nath,[1,3,§] and Sushant K. Raut[4,‖]

[1]*Physical Research Laboratory, Navrangpura, Ahmedabad, Gujarat 380 009, India*
[2]*Department of Physics, LNM Institute of Information Technology (LNMIIT), Rupa-ki-Nangal, post-Sumel, via-Jamdoli, Jaipur, Rajasthan 302 031, India*
[3]*Indian Institute of Technology, Gandhinagar, Ahmedabad, Gujarat 382424, India*
[4]*Department of Theoretical Physics, School of Engineering Sciences, KTH Royal Institute of Technology AlbaNova University Center, Roslagstullsbacken 21, 106 91 Stockholm, Sweden*

(Received 7 August 2015; published 14 January 2016)

The three major unknown neutrino oscillation parameters at the present juncture are the mass hierarchy, the octant of the mixing angle θ_{23} and the CP phase δ_{CP}. It is well known that the presence of hierarchy-δ_{CP} and octant degeneracies affects the unambiguous determination of these parameters. In this paper, we show that a comprehensive way to study the remaining parameter degeneracies is in the form of a generalized hierarchy-θ_{23}-δ_{CP} degeneracy. This is best depicted as contours in the test ($\theta_{23} - \delta_{CP}$) plane for different representative true values of parameters. We show that the wrong-hierarchy and/or wrong-octant solutions can be further classified into eight different solutions depending on whether they occur with the wrong or right value of δ_{CP}. These eight solutions are different from the original eightfold degenerate solutions and can exist, in principle, even if θ_{13} is known. These multiple solutions, apart from affecting the determination of the true hierarchy and octant, also affect the accurate estimation of δ_{CP}. We identify which of these eight different degenerate solutions can occur in the test ($\theta_{23} - \delta_{CP}$) parameter space, taking the long-baseline experiment NOνA running in the neutrino mode as an example. The inclusion of the NOνA antineutrino run removes the wrong-octant solutions appearing with both right and wrong hierarchy. Adding T2K data to this resolves the wrong hierarchy-right octant solutions to a large extent. The remaining wrong-hierarchy solutions can be removed by combining NOνA + T2K with atmospheric neutrino data. We demonstrate this using ICAL@INO as the prototype atmospheric neutrino detector. We find that the degeneracies can be resolved at the 2σ level by the combined data set, for the true parameter space considered in the study.

DOI: 10.1103/PhysRevD.93.013013

I. INTRODUCTION

The standard three-flavor neutrino oscillation probability is described by six parameters, namely three mixing angles (θ_{12}, θ_{23}, θ_{13}), two mass squared differences [Δm^2_{31}, Δm^2_{21} ($\Delta m^2_{ij} = m^2_i - m^2_j$)] and the Dirac CP phase δ_{CP}. The neutrino oscillation data from solar, atmospheric, reactor and accelerator experiments have so far given information about each of these oscillation parameters except δ_{CP} [1–3]. At present, the unknowns in neutrino oscillation physics are (i) the sign of Δm^2_{31} [$\Delta m^2_{31} > 0$ known as normal hierarchy (NH) and $\Delta m^2_{31} < 0$ known as inverted hierarchy (IH)], (ii) the octant of θ_{23} [$\theta_{23} > 45°$ known as a higher octant (HO) and $\theta_{23} < 45°$ known as a lower octant (LO)] and (iii) the CP phase δ_{CP}; any value of this parameter other than 0° and ±180° would signal CP violation in the lepton sector. In this case, it is often useful to talk in terms of the lower half-plane (LHP) with $-180° < \delta_{CP} < 0°$ and upper half-plane (UHP) with $0° < \delta_{CP} < 180°$.

The appearance channel $P_{\mu e}$ often known as the "golden channel" can measure all the three unknown parameters described above.[1] However, the measurement is complicated by the fact that different sets of values of parameters can give the same oscillation probability. This gives rise to degeneracies that render an unambiguous determination of true parameters difficult. It was discussed in Ref. [4] that there can be eight-fold degeneracies in neutrino oscillation probabilities which are (a) the intrinsic or $\theta_{13} - \delta_{CP}$ degeneracy [5], (b) the hierarchy-δ_{CP} degeneracy [6] and (c) the intrinsic octant degeneracy [7]. The intrinsic degeneracy refers to clone solutions occurring due to a different θ_{13} and δ_{CP} value. This degeneracy can be removed to a large extent by using spectral information [8]. Moreover, the current precision determination of θ_{13}

*monojit@prl.res.in
†pomita.ghoshal@gmail.com
‡sruba@prl.res.in
§newton@prl.res.in
‖raut@kth.se

[1]Originally, $P_{\mu e}$ was termed as the golden channel because of its sensitivity to θ_{13}, hierarchy and δ_{CP}.

[9–12] has removed this degeneracy to a great extent. The hierarchy-δ_{CP} degeneracy leads to wrong-hierarchy solutions occurring for a different value of δ_{CP} other than the true value. The intrinsic octant degeneracy refers to duplicate solutions occurring for θ_{23} and $\pi/2 - \theta_{23}$.

Many papers have discussed possibilities of the resolution of these degeneracies by using different detectors in the same experiment [13–15]. The synergistic combination of data from different experiments was also discussed as an effective means of removing such degeneracies by virtue of the fact that the oscillation probabilities offer different combinations of parameters at varying baselines and energies [8,16–23]. In particular, the synergy between long-baseline (LBL) experiments NOνA and T2K in resolving the hierarchy-δ_{CP} degeneracy has been discussed recently in Refs. [24–27].

It has been shown in Refs. [21,28,29] that a precise measurement of the mixing angle θ_{13} is helpful for the removal of octant degeneracy. Octant sensitivity in the T2K and NOνA experiments has been studied recently in Refs. [30,31] in view of the measurement of a nonzero θ_{13}. The octant degeneracy is different for neutrinos and antineutrinos, and hence a combination of these two data sets can be conducive for the removal of this degeneracy for most values of δ_{CP} [32–34].

Since atmospheric neutrino baselines experience strong Earth matter effects, these effectively remove the overlap between right- and wrong-hierarchy solutions [35–38]. In particular, atmospheric neutrino experiments capable of distinguishing neutrinos and antineutrinos can be very useful in resolving degeneracies related to the mass hierarchy [38–48]. The octant sensitivity of the atmospheric neutrinos comes from both the appearance [49] and disappearance channels [50] and also benefits from significant matter effects, especially facilitated by the large value of θ_{13} measured by reactor experiments. Atmospheric neutrinos also provide a synergy with LBL experiments in terms of probability behavior with respect to parameters, so that the combination of atmospheric neutrino data with LBL data exhibits a reduced effect of the hierarchy and octant degeneracies [31,45,51–53].

Recently, it has been realized that for the appearance channel, the octant degeneracy can be generalized to the octant-δ_{CP} degeneracy corresponding to any value of θ_{23} in the opposite octant [31,54]. A continuous generalized degeneracy in the three-dimensional $\theta_{23} - \theta_{13} - \delta_{CP}$ plane has been studied in Ref. [54]. In this work, we show that with the high precision measurement of θ_{13} by reactor experiments, the degeneracies can be discussed in an integrated manner in terms of a generalized hierarchy-$\theta_{23} - \delta_{CP}$ degeneracy. A good way to visualize the different degenerate solutions is in terms of contours in the test $(\theta_{23} - \delta_{CP})$ plane for different choices of true values of parameters.[2] These plots also give an indication regarding the precision of the parameters δ_{CP} and θ_{23}. Although hierarchy degeneracy is discrete, the $\theta_{23} - \delta_{CP}$ degeneracy is continuous for the appearance channel probability $P_{\mu e}$. Inclusion of the information from the disappearance channel $P_{\mu\mu}$ restricts θ_{23}, and discrete degenerate solutions are generated. We classify, for the first time, the wrong-hierarchy and wrong-octant solutions with respect to right or wrong δ_{CP} values. This also allows us to understand how the hierarchy and octant degeneracies can affect the precision in δ_{CP}. We observe that since the wrong-hierarchy and wrong-octant solutions can occur for wrong values of δ_{CP} as well, there can exist, in principle, a total of eight degenerate solutions corresponding to different combinations of hierarchy, octant and δ_{CP}. This is summarized in Table I.[3] Note that these solutions are different from the eight-fold degenerate solutions that have been discussed in the literature. To the best of our knowledge, the parameter degeneracies have not been studied in this generalized form in the literature prior to this. We identify which degenerate solutions among the eight possibilities listed in Table I exist in the neutrino oscillation probabilities for typical baselines and energies corresponding to the LBL experiments T2K and NOνA.

TABLE I. Various possibilities of degeneracy in the probability $P_{\mu e}$. Here, R = right, W = wrong, H = hierarchy and O = octant.

Solution with right δ_{CP}	Solution with wrong δ_{CP}
I. RH-RO-Rδ_{CP}	V. WH-WO-Wδ_{CP}
II. RH-WO-Rδ_{CP}	VI. RH-RO-Wδ_{CP}
III. WH-RO-Rδ_{CP}	VII. RH-WO-Wδ_{CP}
IV. WH-WO-Rδ_{CP}	VIII. WH-RO-Wδ_{CP}

For representative true values of these parameters, we demonstrate to what extent the degenerate solutions can be removed by NOνA, NOνA + T2K and NOνA + T2K+ ICAL. Note that, although the combined capability of NOνA, T2K and ICAL in the hierarchy octant and δ_{CP} determination have been investigated, a comprehensive study for the removal of degeneracies using these three facilities together has not been done before.

The paper is organized as follows. In Sec. II, we give the experimental details of the LBL and atmospheric neutrino experiments being considered. In Sec. III, first we summarize the parameter degeneracies and identify degenerate solutions at the level of neutrino oscillation probabilities. Then, we show their occurrence at the event level considering NOνA and discuss the resolution of the different kinds of degeneracies by combinations of the given

[2]Note that prior to the discovery of a nonzero value of θ_{13}, the degeneracies were studied mainly in $\theta_{13} - \delta_{CP}$ plane.

[3]It is to be noted in this connection that if the δ_{CP} precision is not good, then there can be continuous regions connecting right and wrong δ_{CP} solutions, and hence it may not always be possible to identify discrete wrong δ_{CP} solutions.

experiments. We also present the precision of the parameters θ_{23} and δ_{CP} from the combined analysis with NOνA + T2K + ICAL data. The conclusions are presented in Sec. IV. The Appendix outlines the synergy between the disappearance and appearance channels and the role of antineutrinos.

II. EXPERIMENTAL DETAILS

We use the GLoBES package [55,56] (along with the required auxiliary files [57,58]) to simulate the data of the two long-baseline neutrino oscillation experiments T2K (Tokai to Kamioka, Japan) and NOνA (NuMI Off-Axis ν_e Appearance, Fermilab). The source to detector distance, L, for T2K is 295 km. In the T2K experiment [59], muon neutrinos are directed from J-PARC, making an off-axis angle of 2.5° toward the Super-Kamiokande detector, which is a Water Čerenkov detector of mass 22.5 kt. T2K has been proposed to run for a total luminosity of 7.8×10^{21} protons on target (POT), and it has already collected 10% of the total data in the neutrino mode. At present it is running in the antineutrino mode, and the first results have been reported [60]. The recently operational NOνA experiment is also sending muon neutrinos through two detectors, one at Fermilab (the near detector) and one in northern Minnesota (the far detector), making an off-axis angle of 0.8° and traveling a distance of 810 km to reach the far detector, which is a 14 kt totally active scintillator detector (TASD). The beam power of NOνA is planned to be 700 kW which corresponds to 6×10^{20} POT/year which will run for $3(\nu) + 3(\bar{\nu})$ years. In our simulation of NOνA data, we considered the reoptimized NOνA set up from Refs. [26,61].

For the simulation of an atmospheric neutrino experiment, we consider a magnetized iron calorimeter detector (ICAL) planned by the India-based Neutrino Observatory (INO), the primary goal of which is to study atmospheric muon neutrinos. ICAL@INO has an advantage over other detectors because it has a magnetic field which allows charge discrimination, thus providing the facility to distinguish between μ^+ and μ^-. Here, we consider the 50 kt detector for ICAL@INO with a runtime of 10 years. In our numerical analysis, we have used constant detector angular and energy resolutions of 10° and 10% respectively and 85% overall efficiency. The muon resolutions from INO simulations can be found in Ref. [62]. We have checked that the constant resolutions used in this paper give results similar to those obtained using resolutions from INO simulation codes [44,45]. In our analysis of atmospheric neutrinos, we used the Gaussian formula to compute the statistical χ^2. Systematic errors are taken into account using the method of pulls [63,64] as outlined in Ref. [42]. We have added a 5% prior on $\sin^2 2\theta_{13}$.

We use the following representative values for the oscillation parameters in our numerical simulation as given in Table II, Refs. [1–3].

TABLE II. Values of neutrino oscillation parameters used in our simulations. Here, the second column gives the true values of the parameters, and the third column represents the parameter range over which we have marginalized the test values.

Oscillation parameters	True value	Test value
$\sin^2 2\theta_{13}$	0.1	0.085–0.115
$\sin^2 \theta_{12}$	0.31	–
θ_{23}	LO = 39°, 42°, HO = 48°, 51°	35°–55°
Δm^2_{21}	7.60×10^{-5} eV^2	–
Δm^2_{31}	2.40×10^{-3} eV^2	$(2.15–2.65) \times 10^{-3}$ eV^2
δ_{CP}	90°, 0°,−90°	−180° to +180°

III. IDENTIFYING DEGENERACIES IN NEUTRINO OSCILLATION PARAMETERS AND THEIR RESOLUTION

For the baselines relevant for the experiments NOνA and T2K, the Earth matter density is in the range $(2.3 - 3.0$ g/cc), well below the matter resonance. Therefore, oscillation probabilities computed assuming constant matter density can be used for these experiments. Such probabilities calculated using perturbative expansion of the small leptonic mixing angle θ_{13} (in terms of s_{13}) and the mass hierarchy parameters $\alpha(\equiv \Delta m^2_{21}/\Delta m^2_{31})$ are given as follows [65–67],

$$P_{\mu\mu} = 1 - \sin^2 2\theta_{23} \sin^2 \Delta + \mathcal{O}(\alpha, s_{13}) \tag{1}$$

$$\begin{aligned} P_{\mu e} = {} & 4 s^2_{13} s^2_{23} \frac{\sin^2 (A-1)\Delta}{(A-1)^2} + \alpha^2 \cos^2\theta_{23} \sin^2 2\theta_{12} \frac{\sin^2 A\Delta}{A^2} \\ & + \alpha s_{13} \sin 2\theta_{12} \sin 2\theta_{23} \cos(\Delta + \delta_{cp}) \\ & \times \frac{\sin(A-1)\Delta}{(A-1)} \frac{\sin A\Delta}{A}, \end{aligned} \tag{2}$$

where $s_{ij}(c_{ij}) = \sin\theta_{ij}(\cos\theta_{ij})$ for $j > i$ $(i, j = 1, 2, 3)$. We use the following notation: $\Delta \equiv \Delta m^2_{31} L/4E$, $A \equiv 2EV/\Delta m^2_{31} = VL/2\Delta$, where $V = \sqrt{2} G_F n_e$ is the Wolfenstein matter term. The antineutrino oscillation probability can be obtained by replacing $\delta_{CP} \to -\delta_{CP}$ and $V \to -V$. Hence, in the neutrino oscillation probability, A is positive for NH and negative for IH, and for antineutrinos, the sign of A gets reversed. We observe the following salient features from the probability formulas:

(i) The leading order term in the muon neutrino survival probability $P_{\mu\mu}$, also known as the disappearance channel, is proportional to $\sin^2 2\theta_{23} \sin^2 \Delta$. This gives rise to the intrinsic hierarchy and octant degeneracies:

$$P_{\mu\mu}(\Delta) = P_{\mu\mu}(-\Delta) \tag{3}$$

$$P_{\mu\mu}(\theta_{23}) = P_{\mu\mu}(\pi/2 - \theta_{23}). \tag{4}$$

This leads to a loss of sensitivity to the hierarchy and octant, when the measurement is performed using this channel.

(ii) The appearance channel $P_{\mu e}$ does not have intrinsic degeneracies but suffers from the combined effect of different parameters, which leads to the following set of degeneracies:

$$P_{\mu e}(\theta_{13}, \delta_{CP}) = P_{\mu e}(\theta'_{13}, \delta'_{CP}) \tag{5}$$

$$P_{\mu e}(\Delta, \delta_{CP}) = P_{\mu e}(-\Delta, \delta'_{CP}). \tag{6}$$

Equations (4)–(6) constitute the eight-fold degeneracy discussed in Ref. [4].

Recently, it has been discussed that in the context of probabilities which are dependent on $\sin^2\theta_{23}$, the octant degeneracy can be generalized to include all values of θ_{23} in the second octant [31] and can also be correlated with δ_{CP} [31,68]. The pattern of parameter degeneracies in the three-dimensional $\theta_{23} - \theta_{13} - \delta_{CP}$ space arising from the appearance probability $P_{\mu e}$ has been discussed in Ref. [54]. This is a continuous degeneracy and can be expressed as

$$P_{\mu e}(\theta_{23}, \theta_{13}, \delta_{CP}) = P_{\mu e}(\theta'_{23}, \theta'_{13}, \delta'_{CP}) \Rightarrow \text{generalized octant degeneracy.} \tag{7}$$

However, the reactor experiments have measured $\sin^2\theta_{13}$ with a high degree of accuracy, and future measurements are expected to improve it further. This has reduced the impact of θ_{13} uncertainty on octant degeneracy to a large extent [31]. In this paper, we consider another generalized degeneracy which is the hierarchy-$\theta_{23} - \delta_{CP}$ degeneracy:

$$P_{\mu e}(\theta_{23}, \Delta, \delta_{CP}) = P_{\mu e}(\theta'_{23}, -\Delta', \delta'_{CP}) \Rightarrow \text{generalized hierarchy} - \theta_{23} - \delta_{CP} \text{ degeneracy.} \tag{8}$$

This degeneracy can be observed best in the test $\theta_{23} - \delta_{CP}$ plane. Studying it in this fashion allows us to view the degeneracies arising out of the remaining unknown parameters in a comprehensive manner. We note that while the hierarchy degeneracy is always discrete, the $\theta_{23} - \delta_{CP}$ degeneracy arising out of the appearance channel is continuous. On the other hand, the intrinsic octant degeneracy arising from the $P_{\mu\mu}$ channel is independent of δ_{CP} and discrete in θ_{23} except for θ_{23} values close to maximal. Thus, combining the survival and conversion probabilities gives rise to disconnected degenerate regions in the $\theta_{23} - \delta_{CP}$ plane. We have elaborated on this point in the Appendix.

In the next subsection, we study the occurrence of the above degeneracies in terms of probabilities for NOνA and T2K and identify the different possible degenerate solutions at the probability level.

A. Identifying degeneracies at the probability level

Figure 1 shows the probability $P_{\mu e}$ for neutrinos (left panel) and antineutrinos (right panel) as a function of δ_{CP} for both NH and IH. The plots in the upper panel correspond to NOνA, while those in the lower panel are for T2K. These probabilities are plotted for the energy where the neutrino flux peaks. The hatched area denotes variation over θ_{23}. For the lower (higher) octant, we vary θ_{23} between 39°–42° (48°–51°). This is a good assumption for θ_{23} not too close to its maximal value, for the purpose of illustrating the physics, since for a given θ_{23}(true), the disappearance channel anyway excludes values away from θ_{23}(true) and $\pi/2 - \theta_{23}$(true). Thus, these plots implicitly assume information from the disappearance channel. From Fig. 1, the following points can be noted:

For neutrinos—

(i) The NH probabilities are higher than the IH probabilities. This is because of the enhanced matter effect for neutrinos for NH in the Earth's matter.

(ii) For both NH and IH, the probabilities are higher in the LHP.

(iii) The probabilities for a higher octant are higher for both NH and IH.

While, for antineutrinos—

(i) "A" changes its sign, and IH probabilities become higher than NH.

(ii) The flip in sign of δ_{CP} makes both the NH and IH probabilities higher in the UHP.

(iii) Like neutrinos, the probabilities for a higher octant remain higher for both NH and IH. For both neutrinos and antineutrinos, the lowest line in the LO (HO) band corresponds to 39° (48°), while the highest point corresponds to 42° (51°), due to the $\sin^2\theta_{23}$ dependence of the leading order term.

The overlapping regions between various curves at a specific value of δ_{CP} indicate the degeneracy occurring *for the right value of* δ_{CP}, while the same value of the probability for different δ_{CP} values denotes degeneracy occurring *at wrong values of* δ_{CP}. Clearly, the former would correspond to solutions with the wrong hierarchy and/or octant with right δ_{CP}, while the latter would correspond to the solutions with the wrong hierarchy and/or octant and wrong δ_{CP}. The wrong-CP degenerate solutions corresponding to a given true value of θ_{23} and δ_{CP} can be obtained from the probability figures by drawing a horizontal line through this point. The different intersection points of this line with the probability bands are degenerate as they share the same value of probability. However, the degenerate solutions occurring for a particular θ_{23} (true) which is not in the vicinity of $\pi/2 - \theta_{23}$ (true) in the opposite octant will be excluded by the disappearance channel, and the occurrence of these solutions in the test $\theta_{23} - \delta_{CP}$ plane will depend on the θ_{23} precision of the disappearance channel.

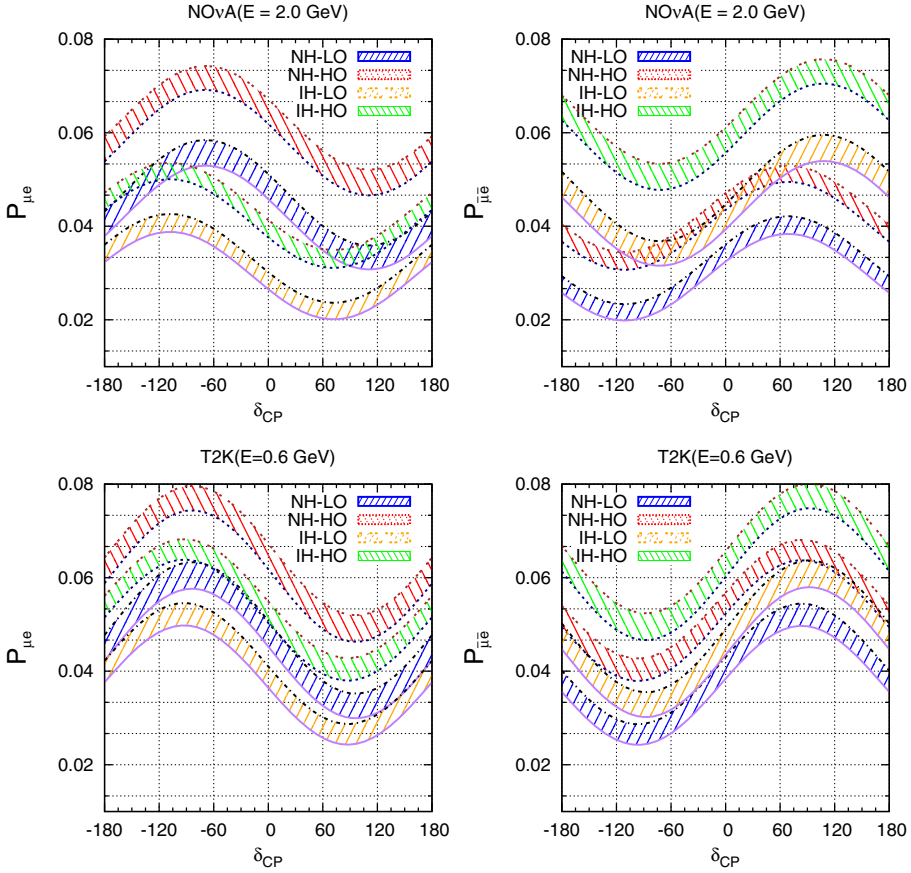

FIG. 1. The oscillation probability $P_{\mu e}$ as a function of δ_{CP}. Here, the upper row represents oscillation probability for NOνA [L = 810 km], and the lower row represents probability for T2K [L = 295 km]. The left panel is for neutrinos, while the right panel is for antineutrinos.

Below, we explain the occurrence of the different degenerate combinations of $\{\text{hierarchy}, \theta_{23}, \delta_{CP}\}$ taking the NOνA neutrino probabilities (the top-left panel) as reference unless otherwise mentioned:

(1) The overlapping regions between the NH-LO (blue) and IH-HO (green) bands around $\delta_{CP} = -120°$ and 90° give rise to WH-WO-Rδ_{CP} degenerate solutions in the probability. However, for antineutrinos, these bands are well separated. Thus, combining NOνA neutrino and antineutrino data can help in removing these solutions.

(2) The probability corresponding to UHP of the NH-LO (blue) band can be the same as those for the LHP of the IH-LO (yellow) band for $\theta_{23} = 39°$. This can give rise to WH-RO-Wδ_{CP} solutions. Note that this degeneracy is present in the antineutrinos for the same values of δ_{CP}. Thus, for true NH, UHP (i.e. $0° < \delta_{CP} < 180°$) is the unfavorable half-plane of δ_{CP}, and this degeneracy cannot be resolved by using NOνA data alone. For T2K, the probability exhibits a sharper variation with δ_{CP}, and hence this degeneracy is less pronounced between the UHP and LHP. Hence, the addition of T2K data to NOνA can be helpful in removing this degeneracy. For LHP (i.e. $-180° < \delta_{CP} < 0°$), which is the favorable half-plane of δ_{CP} in NH, there is no WH-RO-Wδ_{CP} solution for both NOνA and T2K.

(3) For $\delta_{CP} \in$ UHP, the NH-HO (red) band can share same value of probability with NH-LO (blue) band for $\delta_{CP} \in$ LHP. This is the reason for the RH-WO-Wδ_{CP} solution. For antineutrinos, the degeneracy is seen to be between NH-HO-LHP and NH-LO-UHP. Thus, a combination of neutrinos and antineutrinos helps to remove this degeneracy.

(4) The WH-WO-Wδ_{CP} solution can be observed along the isoprobability line that intersects the NH-LO (blue) and IH-HO (green) bands at different values of δ_{CP}. This degeneracy can be seen for instance between $\{\text{NH}, 39°, -180°\}$ and $\{\text{IH}, 51°, 0°\}$. Again, the antineutrino probability does not suffer from this degeneracy, and thus combining neutrino and antineutrino data can be helpful in removing these solutions.

(5) One can also have RH-RO-Wδ_{CP} solutions as a result of a so-called "intrinsic *CP* degeneracy" that occurs for the same hierarchy and same value of θ_{23} but at a different value of δ_{CP}. This is due to the

harmonic dependence of the probability on δ_{CP}. For instance, within the NH-HO (blue) band, $\delta_{CP} = 0°$ and $\delta_{CP} \approx -135°$ have the same value of probability for $\theta_{23} = 39°$. However, for antineutrinos, this occurs for $\delta_{CP} = 0°$ and $\delta_{CP} = +135°$. Thus, a combination of neutrino and antineutrino data can help to get rid of this degeneracy. This can also be seen to occur for T2K, for$\{\text{NH}, 48°, -180°\}$ and $\{\text{NH}, 48°, 0°\}$. For T2K, since the flux peak coincides with the probability peak, the CP-dependent term is proportional to $\sin\delta_{CP}$, and thus this degeneracy occurs for δ_{CP} and $\pi - \delta_{CP}$ [68]. For NOνA, since the flux and the probability peak are not at the same energy, the degeneracy does not correspond exactly to δ_{CP} and $\pi - \delta_{CP}$. It is interesting to note that this degeneracy does not occur for $\delta_{CP} = \pm 90°$.

Thus, among the eight solutions listed above, only the WH-RO-Rδ_{CP} and RH-WO-Rδ_{CP} solutions do not exist even at the probability level. The above description is in terms of probabilities without including any experimental errors. At the event level, many of these may not appear as discrete degeneracies. In particular, for a C.L. beyond the reach of a particular experiment's precision, the different discrete degenerate solutions merge, and the degeneracy becomes continuous.

Note that another way to understand the degeneracies is the biprobability ellipses in the $P_{\mu e} - P_{\bar{\mu}\bar{e}}$ plane [6]. This requires a single plot for neutrinos and antrineutrinos. However, each point on these ellipses corresponds to different values of δ_{CP} which cannot be read off from the plots. The probability band plots presented in this paper provide a complementary way to visualize the occurrence of the degeneracies at different CP values, and one can readily identify the wrong and right δ_{CP} solutions which are the main focus of this work.

B. Identifying degeneracies at the event level

To show the occurrence of the different degeneracies at the event level, in Fig. 2 we present a set of contour plots in the $\theta_{23} - \delta_{CP}$ test-parameter plane assuming only neutrino run (6 years) of NOνA, which is denoted as $[6 + 0]$. We note that the proposed run time of NOνA is $3 + 3$. However, in this section, we intend to identify which of the different degenerate solutions discussed in Table I can arise in the $\theta_{23} - \delta_{CP}$ plane. Since the wrong-octant solutions disappear including the antineutrino run, the $6 + 0$ case is the best option for visualizing all the possible degenerate solutions. The $3 + 3$ case is discussed in the next section. These sets of plots also show the role of statistics which can give enhanced precision *vis-à-vis* the antineutrino run which helps in resolving degeneracies. Similar plots can also be drawn for the T2K $8 + 0$ case. However, for T2K, since the hierarchy sensitivity is much less, the possibility of getting continuous regions instead of discrete degenerate solutions is more. Thus, the different degenerate solutions cannot be visualized so distinctly, and in this section, our main aim is to identify the different degenerate solutions in the $\theta_{23} - \delta_{CP}$ plane. This can be done better with NOνA $6 + 0$ as the illustrative example. These plots are drawn assuming true hierarchy to be NH and different choices of true values of θ_{23} and δ_{CP}. In this and all the other subsequent figures, the successive rows are for $\theta_{23} = 39°$, 42°, 48°, 51°. The true δ_{CP} values chosen are $\pm 90°$ corresponding to maximum CP violation and 0° corresponding to CP conservation. The blue contours correspond to the right hierarchy, and magenta curves correspond to the wrong hierarchy.

The first column of Fig. 2 shows the degenerate solutions for $\delta_{CP} = -90°$ for NOνA running only in the neutrino mode. For $\theta_{23} = 39°$, apart from the true solution, RH-WO-Wδ_{CP} and WH-WO-Rδ_{CP} solutions are observed in the upper and lower right quadrants respectively. The RH-WO-Wδ_{CP} solution is also seen for $\theta_{23} = 42°$. For this case, at $\delta_{CP} = -90°$, the uppermost point of the blue band in the NOνA neutrino probability, in Fig. 1 one can see that the same value of probability is possible for NH-HO (red band) near $\delta_{CP} = +45°$ and $\pm 180°$. This explains the shape of the allowed zone—wider at these values and narrower at 90°. The WH-WO-Rδ_{CP} solution is seen only at a 2σ level for $\theta_{23} = 42°$. This can be understood by observing that the points 42° (the upper tip of the blue band) and 48° (the lower tip of the green band) are more separated as compared to 39° (the lower tip of the blue band) and 51° (the upper tip of the green band). For θ_{23} in the higher octant (48° and 51°), there are no spurious wrong-hierarchy solutions even with only neutrinos. This is because for NH, θ_{23} in the higher octant and −90° correspond to the maximum probability for neutrinos, and this cannot be matched by any other combination of parameters. Hence, no degenerate solutions appear, and only the neutrino run for NOνA suffices to give an allowed area only near the true point. Note that the contours for 48° extend to the wrong octant also. However, (here and elsewhere) this is not due to any degenerate behavior of the $P_{\mu e}$ probability but due to the poor θ_{23} precision of the $P_{\mu\mu}$ channel near maximal mixing.

The second column represents $\delta_{CP} = +90°$. In this case, we observe a WH-WO-Rδ_{CP} solution for both $\theta_{23} = 39°$ and 42°. This can be understood from the intersection of the blue and green bands in Fig. 1 close to $\delta_{CP} = 90°$ in the UHP. We also get a WH-RO-Wδ_{CP} region in the LHP. For 42°, since the θ_{23} precision coming from the disappearance channel is worse, at 2σ both these solutions merge, and a discrete degenerate region is not obtained. For $\theta_{23} = 51°$ from Fig. 1, we see that the point $\{\text{NH}, +90°, 51°\}$ in the red band intersects the blue band around $\{\text{NH}, -90°, 39°\}$ giving a RH-WO-Wδ_{CP} solution.

A WH-RO-Wδ_{CP} solution is also obtained in this case in the LHP. Similar regions are also obtained for $\theta_{23} = 48°$.

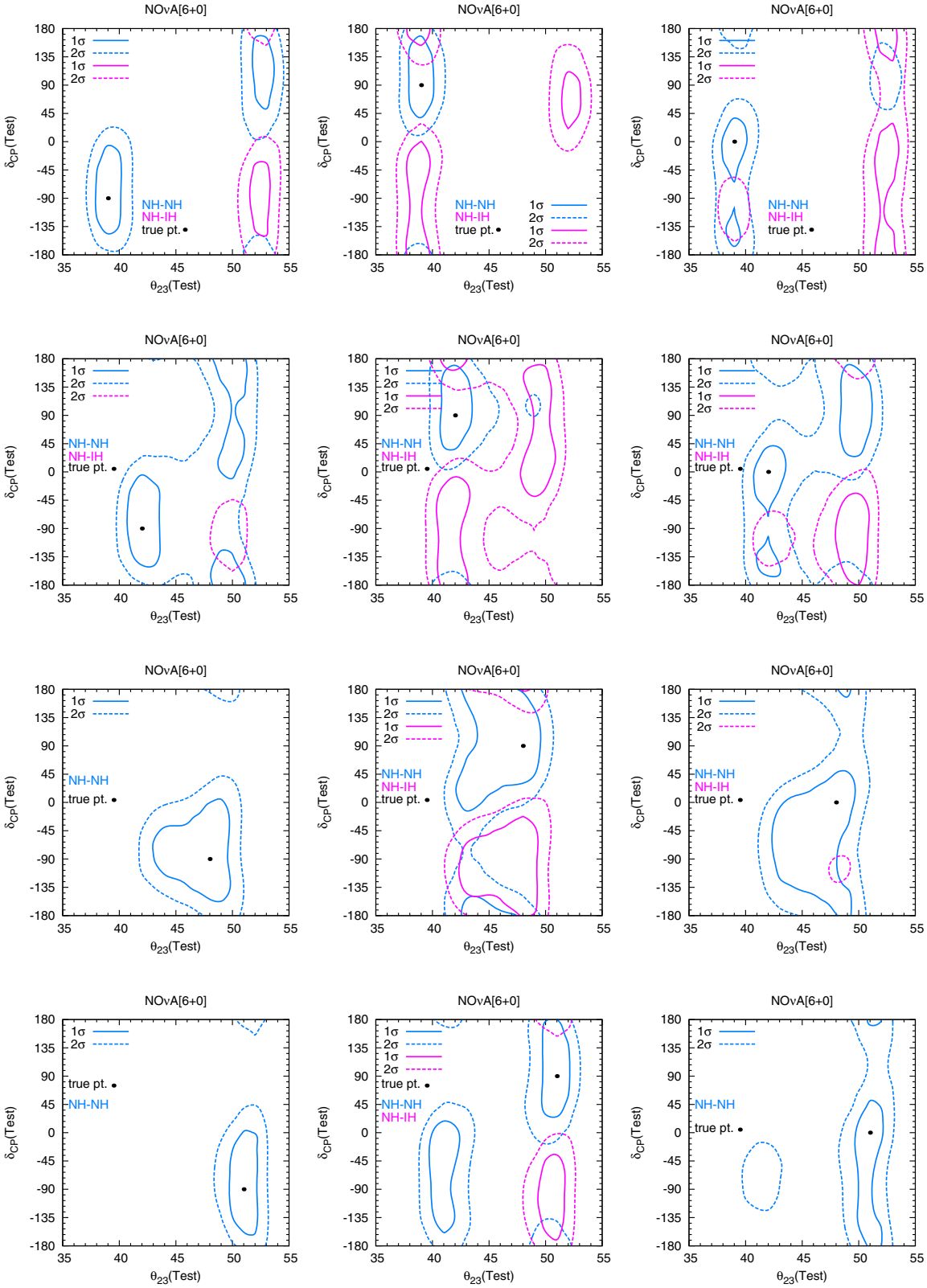

FIG. 2. Contour plots for NOνA$[6+0]$ with true values of $\theta_{23} = 39°, 42°, 48°, 51°$ in successive rows. The three columns correspond to $\delta_{CP} = -90°$, 90°, 0° respectively.

However, the RH-WO-Wδ_{CP} solution merges with the true solution at 2σ level.

For $\delta_{CP} = 0°$, a discrete RH-RO-Wδ_{CP} solution is seen to be allowed at 1σ for $\theta_{23} \in$ LO. This is due to the intrinsic CP degeneracy as discussed in the context of probabilities. But at 2σ, due to the poor δ_{CP} precision, this degeneracy becomes continuous, and the whole LHP becomes allowed. For θ_{23} belonging to the higher octant, larger statistical errors are involved as compared to $\theta_{23} \in$ LO, and this degeneracy appears as continuous in the LHP even at 1σ, and at 2σ the full δ_{CP} range becomes allowed. For $\theta_{23} = 39°$ and 42°, we also see wrong-hierarchy solutions appearing in the wrong octant. From the probability figure, we identify that this degeneracy occurs around $\delta_{CP} = -30°, -180°, 180°$ for $\theta_{23} = 39°$ which allows the LHP of δ_{CP} at 1σ and the whole δ_{CP} range at 2σ. For $\theta_{23} = 42°$, this degeneracy is seen to occur around $\delta_{CP} = -90°$ giving distinct degenerate solutions at the 1σ and 2σ levels. For $\theta_{23} = 42°$, a discrete RH-WO-Wδ_{CP} solution appears at 1σ. From Fig. 1, it is seen that $\{\text{NH}, 42°, 0°\}$ has the same value of probability corresponding to $\{\text{NH}, 48°, 90°\}$. At 2σ, this merges with the RH-RO-Wδ_{CP} solution. For $\theta_{23} = 39°$, this solution appears as a 2σ allowed patch around $\{\text{NH}, 51°, 90°\}$. From Fig. 1, it can be seen that the above points are not exactly degenerate in terms of probability, but due to lack of precision, they become allowed. For a similar reason, the 2σ patch with wrong hierarchy appears in the right octant for $\theta_{23} = 39°$ and 42°. For $\theta_{23} = 51°$, a right-hierarchy patch occurs with the wrong octant. For $\theta_{23} = 48°$, because of the proximity to maximal mixing, the true parameter space also extends to the wrong octant. In general, we see that the CP precision is poorer for $\delta_{CP} = 0°$ at this stage. This is due to the unresolved degeneracies for $\delta_{CP} = 0°$ which lead to multiple allowed regions and continuous bands at 2σ.

C. Successive resolution of degeneracies with data from different experiments

In this section, first we show the status of the above degenerate regions when NOνA runs in [3 + 3] configuration. We then study the combined potential of NOνA[3 + 3] and T2K[8 + 0] in resolving the degeneracies. Finally, we add the atmospheric neutrino data from ICAL and show its impact.

It is well known that due to Earth matter effects and the presence of an antineutrino component in the atmospheric neutrino flux, ICAL can play a prominent role in resolving the hierarchy and octant degeneracies [44,62]. Since there is no δ_{CP} dependence in ICAL, the hierarchy and octant sensitivities are independent of δ_{CP}. This δ_{CP}-independent χ^2 adds to the χ^2 for NOνA and T2K in the degenerate region, and the wrong-hierarchy and wrong-octant solutions can be resolved. This aids in improving both the octant and δ_{CP} sensitivities of T2K and NOνA [31,69,70]. Note that this is a synergistic effect and the combined sensitivity is better than that obtained by adding individual χ^2 values.

The advantage offered by the atmospheric neutrino detector ICAL and the synergy between the various experiments in removing the degeneracies can be seen from these plots. It is noteworthy that the allowed area in the test $\theta_{23} - \delta_{CP}$ plane also gives an idea about the precision of these two parameters.

Our results are presented in Figs. 3–5 which correspond to true $\delta_{CP} = -90°$, 90° and 0° respectively. In each figure, the successive columns represent NOνA[3 + 3], NOνA[3 + 3] + T2K[8 + 0] and NOνA[3 + 3] + T2K[8 + 0] + ICAL respectively. In these figures, the following generic features can be noted:

(i) Comparing with the NOνA[6 + 0] panels, in all the NOνA[3 + 3] figures, we note that the addition of antineutrino information removes the wrong-octant degenerate regions. This also includes the wrong-hierarchy regions occurring with the wrong octant. For $\theta_{23} = 39°$ and 51°, the wrong-octant regions are almost completely removed. But for the true θ_{23} values 42° and 48°, both the right-hierarchy and wrong-hierarchy solutions extend to the wrong-octant region.

(ii) When T2K data is added to NOνA[3 + 3], it helps in removing these wrong-octant extensions. The wrong hierarchy-right octant regions also get significantly reduced in size by adding T2K data to NOνA[3 + 3]. This is due to the fact that for T2K, these solutions occur at different δ_{CP} values than NOνA. Addition of T2K data also improves the precision of θ_{23} and δ_{CP}.

(iii) When ICAL data are added to T2K and NOνA, the remaining wrong-hierarchy regions are resolved for all the true values of θ_{23} considered. The wrong-octant extensions of the right-hierarchy solutions are also reduced in size, and the precision of θ_{23} improves. The combination of T2K + NOνA + ICAL can resolve all the degeneracies at a 2σ level for true $\theta_{23} = 39°$, 51° for all the three δ_{CP} values. For the θ_{23} and δ_{CP} combinations of $\{42°, 0°\}$ and for 48°, ±90°, 0°, there are still allowed regions in the wrong octant. Note that some of the wrong-octant regions that are removed by the NOνA antineutrino run could also be removed by the ICAL data.

Apart from the above features, the following important points can be observed from the figures:

(i) For $\delta_{CP} = -90°$, there are no wrong-hierarchy solutions in NOνA[3 + 3], and the addition of T2K helps in improving the θ_{23} precision. This feature is particularly prominent for $\theta_{23} = 42°$ and 48° where T2K data help in removing the wrong-octant extensions for the right-hierarchy solutions. With the addition of ICAL data, the wrong-octant

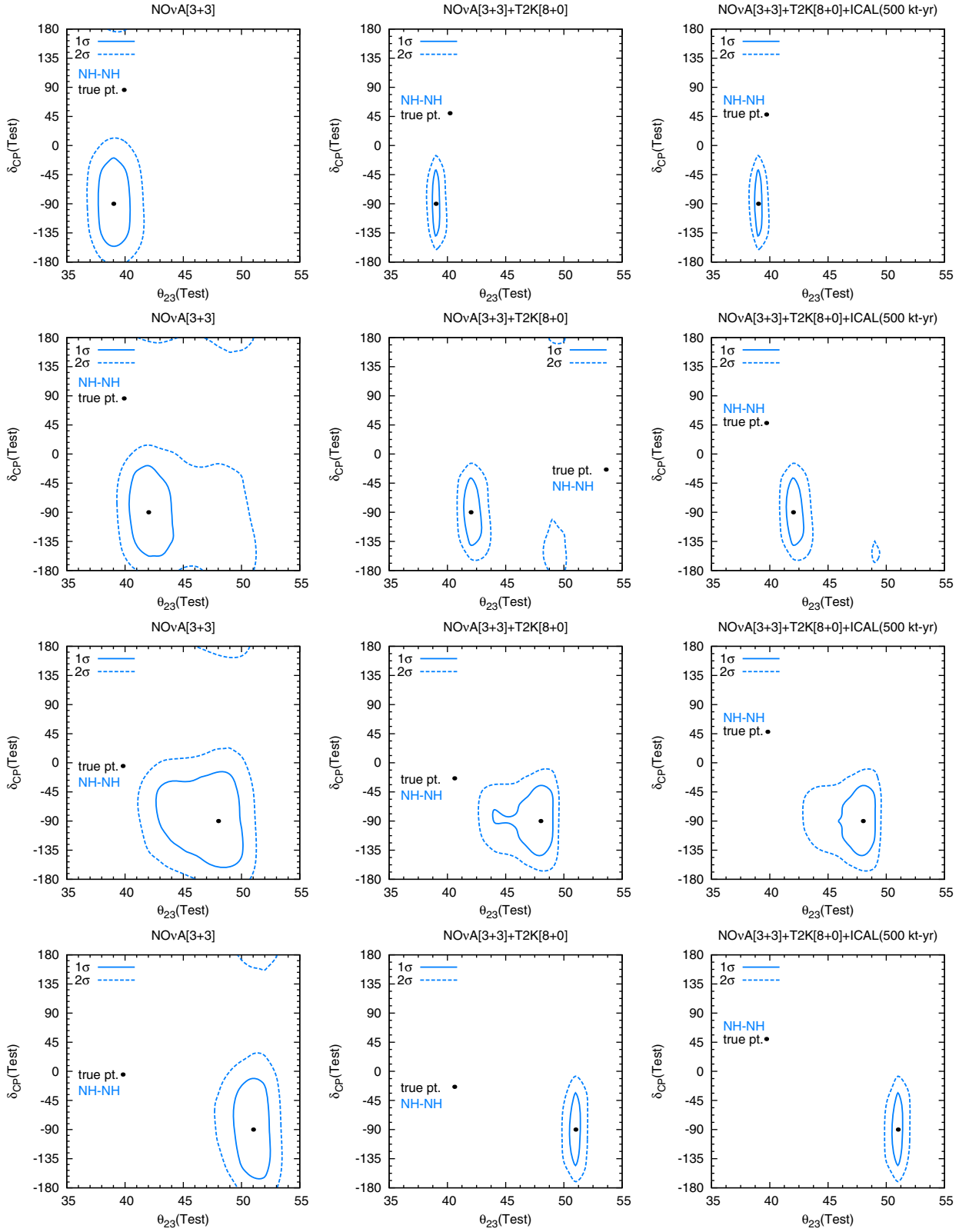

FIG. 3. Contour plots in the test $\theta_{23} - \delta_{CP}$ plane for true $\delta_{CP} = -90°$ and true $\theta_{23} = 39°, 42°, 48°$ and $51°$ in successive rows. The first column is for NOνA$[3+3]$. The second and third columns are for NOνA$[3+3]+$T2K$[8+0]$ and NOνA$[3+3]+$T2K$[8+0]+$ ICAL respectively.

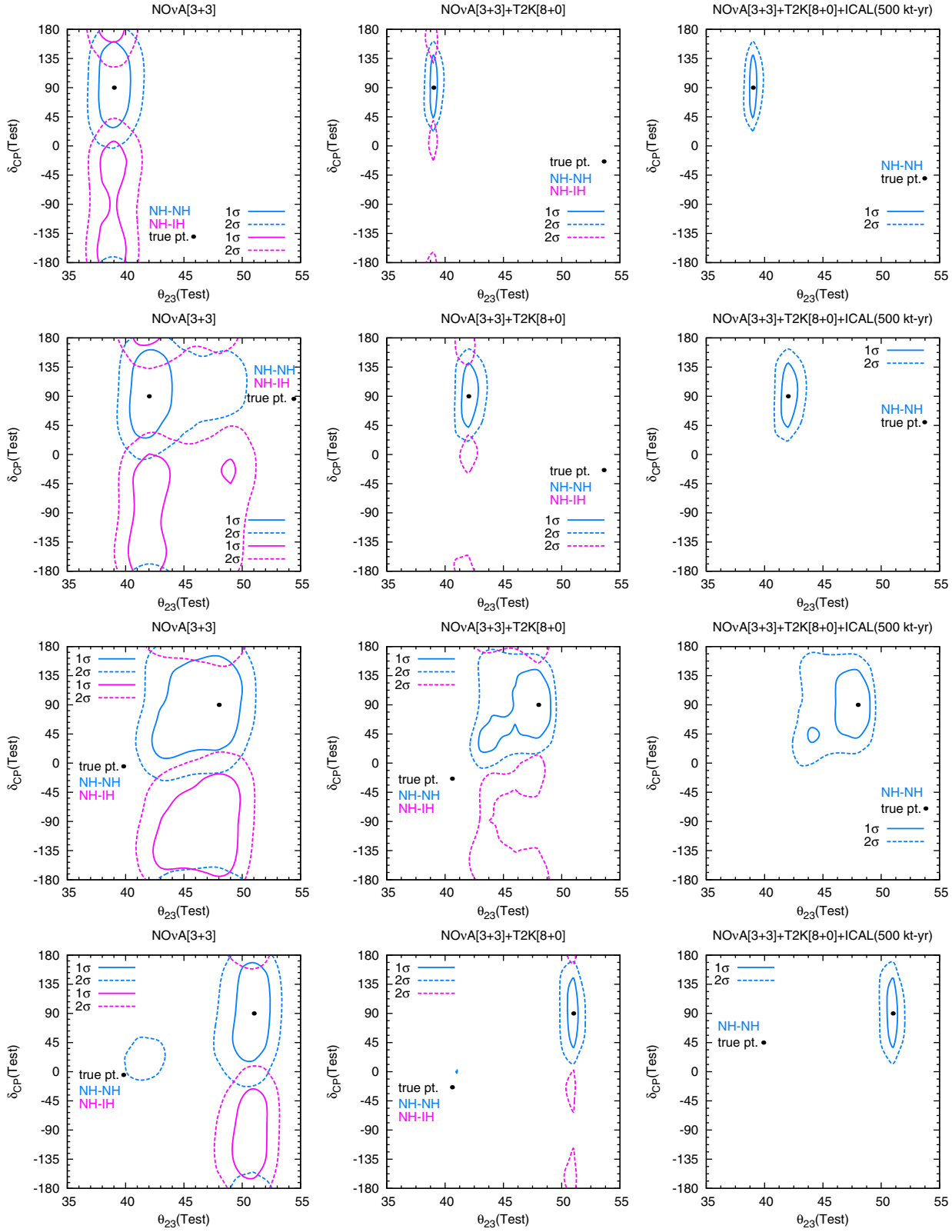

FIG. 4. Same as in Fig. 3 but for true $\delta_{CP} = +90°$.

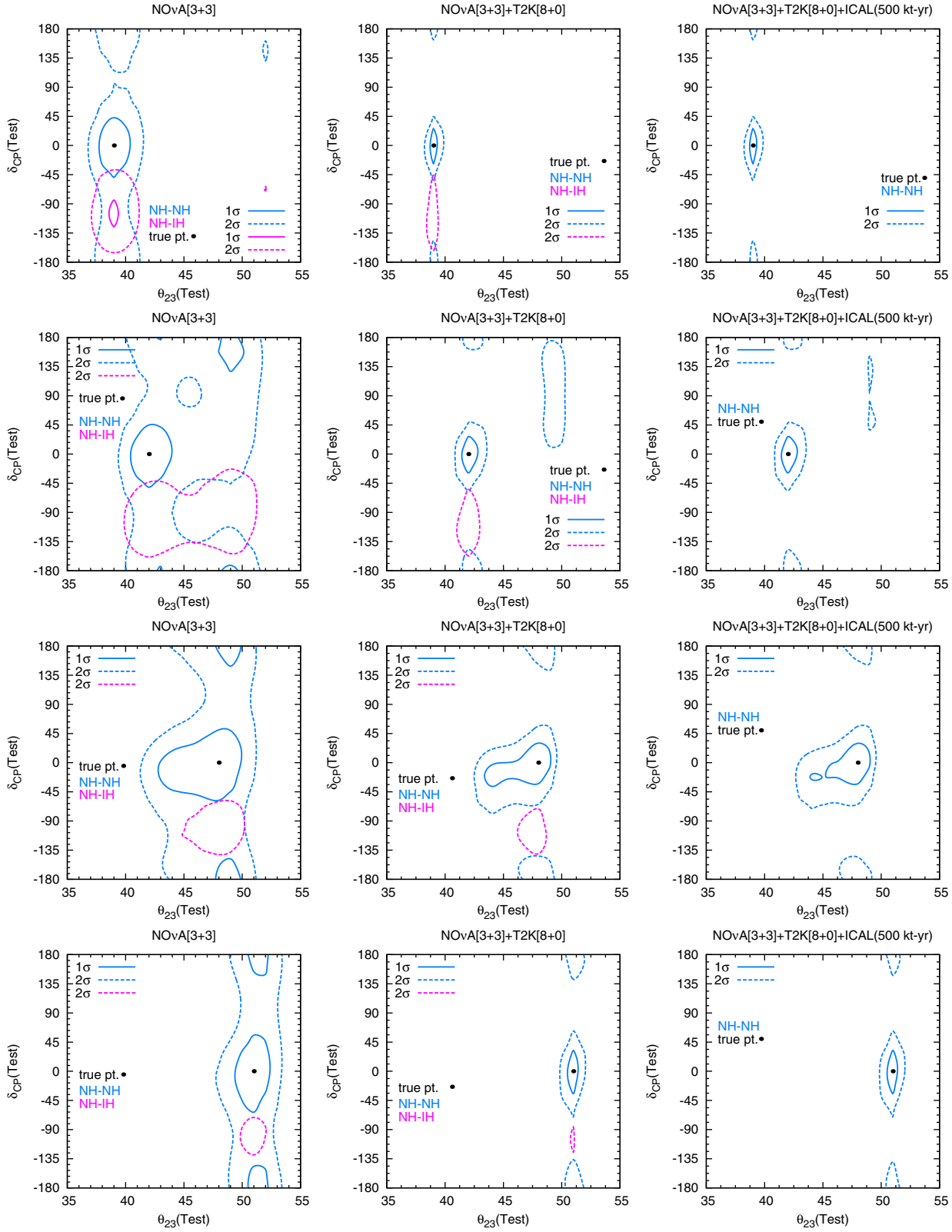

FIG. 5. Same as in Fig. 3 but for true $\delta_{CP} = 0°$.

solution is almost resolved for $\theta_{23} = 42°$, while for $\theta_{23} = 48°$, the same is resolved at 1σ.

(ii) For $\delta_{CP} = -90°$ and $\theta_{23} = 51°$, NOνA can already resolve all the degeneracies with 6 years of neutrino run only as can be seen in Fig. 2. However, the precision of θ_{23} is worse with NOνA$[3+3]$. This is because splitting the neutrino run into equal neutrino and antineutrino runs reduces the statistics, and hence the precision becomes worse.

(iii) For $\delta_{CP} = 90°$, we also see that for $\theta_{23} = 48°$, the wrong-hierarchy region in NOνA$[3+3]$ + T2K$[8+0]$ is still quite large, and this is where ICAL has a remarkable role to play. We see that when ICAL data are added, the large wrong-hierarchy region corresponding to $\theta_{23} = 48°$ completely vanishes.

(iv) The small 1σ wrong hierarchy-wrong octant allowed zone for $\delta_{CP} = 90°$ and $\theta_{23} = 42°$ in NOνA$[3+3]$ can be identified as the part of the WH-WO-Rδ_{CP} solution of NOνA$[6+0]$ by comparing with Fig. 2.

(v) For $\delta_{CP} = 0°$, adding T2K data to NOνA$[3+3]$ improves the precision considerably and also removes the wrong-hierarchy solutions to a large extent. The precision of θ_{23} and δ_{CP} around the true solution also improves. The enhanced precision due to adding T2K is also responsible for reducing the continuous allowed regions to discrete degenerate solutions for θ_{23} values near 45°. Adding ICAL data removes the remaining wrong-hierarchy regions and further help to pinpoint the allowed zones at a 2σ level.

(vi) In NOνA$[3+3]$, for $\delta_{CP} = 0°$ and $\theta_{23} = 39°$, 42°, comparing with the corresponding figures in Fig. 2, we see that the spurious solution appearing at $-150°$ at 1σ due to the intrinsic degeneracy is no longer present with the addition of antineutrino data, since for the antineutrino probability in NOνA the intrinsic degeneracy is between 0° and +150° as discussed earlier. Thus, the addition of neutrino and antineutrino data solves the intrinsic degeneracy at 1σ at both these δ_{CP} values, but at 2σ, both $\pm 150°$ remain allowed. The allowed area near the true value increases in size because replacing half the neutrino run with antineutrinos reduces the statistics, and hence the precision becomes worse.

The following additional observations can be made regarding alternative parameter values and running modes:

(i) In generating the above plots, we considered T2K running in the neutrino mode with its full beam power. We find that once one includes the antineutrino run from NOνA, running T2K in the antineutrino mode is no longer necessary for removing spurious wrong-octant solutions. Rather, running in the neutrino mode gives enhanced statistics and hence better precision. If on the other hand NOνA runs in full neutrino mode and the antineutrino component comes from T2K, we have verified that we get similar results.

(ii) We have presented the results for the case of true NH. If the true hierarchy is chosen to be IH, one would get a different set of allowed regions based on the degeneracies observed in Fig. 1. For example, for $\delta_{CP} = -90°$ and $\theta_{23} = 39°$ for NOνA$[6+0]$ in the true IH case, apart from the true solution, RH-WO-Wδ_{CP} and WH-RO-Wδ_{CP} solutions would be obtained. This can be predicted from Fig. 1 (top left panel) by drawing a horizontal line from the bottom of the IH-LO band at $\delta_{CP} = -90°$, which cuts both the IH-HO and NH-LO bands near $\delta_{CP} = 90°$.

The situation for NOνA$[3+3]$ and other combinations would be more complicated since the allowed regions and precision for true IH depend not only on the probability behavior but also on the statistics of neutrino and antineutrino data in the respective experiments.

(iii) The results are significantly dependent on the true value of θ_{13}, chosen here to be $\sin^2 2\theta_{13} = 0.1$. Lower values of θ_{13} (or worse θ_{13} precision) would lead to poorer CP precision and more difficulty in removing the degeneracies. This is because δ_{CP} is coupled with θ_{13} in the oscillation probability.

D. Distinguishability between 0° and 180°

It will also be interesting to see how far the two CP conserving values 0° and 180° can be distinguished by the experimental setups considered. In this section, we discuss this issue. The true events are generated for $\delta_{CP} = 0°$, $\theta_{23} = 39°$ and normal hierarchy. In the test spectrum, we consider $\delta_{CP} = 180°$ and marginalize over θ_{13}. For purposes of comparison, we also give the results for test $\delta_{CP} = 90°$. The results are presented in Table III. We observe that a 2σ sensitivity in distinguishing between $\delta_{CP} = 0°$ and $\delta_{CP} = 180°$ can be achieved by NOνA + T2K. Adding ICAL data increases the sensitivity further. It is interesting to note that for beam based experiments, 0° and 90° have much larger separation than that between 0° and 180°. But for ICAL, 0° and 180° are more separated though the χ^2 values are very small. This is because ICAL itself has limited CP sensitivity due to angular smearing over all directions [69]. Note that for experiments like PINGU, the CP sensitivity can be

TABLE III. χ^2 sensitivity for test $\delta_{CP} = 90°$, 180° with true $\delta_{CP} = 0°$, true hierarchy as NH and true θ_{23} as 39°.

$\nu + \bar{\nu}$	Test $\delta_{CP} = 90°$	Test $\delta_{CP} = 180°$
NOνA$[3+3]$	6.31	2.82
NOνA$[3+3]$ + T2K$[8+0]$	14.63	4.77
ICAL	1.21	1.60
NOνA$[3+3]$ + T2K$[8+0]$ +ICAL	14.83	5.4

TABLE IV. Percentage precision of parameters θ_{23} and δ_{CP} around the true value using NOνA + T2K + ICAL.

True value		LO precision				True value		HO precision			
θ_{23}	δ_{CP}	1σ		2σ		θ_{23}	δ_{CP}	1σ		2σ	
		θ_{23}	δ_{CP}	θ_{23}	δ_{CP}			θ_{23}	δ_{CP}	θ_{23}	δ_{CP}
39°	+90°	1.02	26.63	2.17	39.50		+90°	3.15	28.45	7.70	48.27
	−90°	0.89	34.52	2.17	41.52	48°	−90°	3.15	30.00	7.35	43.22
	0°	0.64	15.83	2.04	28.33		0°	4.03	17.50	7.59	35.80
42°	+90°	1.6	27.00	3.32	38.52		+90°	0.88	30.32	2.16	43.33
	−90°	1.7	29.77	3.31	41.52	51°	−90°	0.98	34.48	2.16	45.00
	0°	1.66	15.83	3.08	29.16		0°	0.88	19.16	2.16	37.50

higher, and the χ^2 difference between 0° and 180° can be appreciable [71].

E. Precision of θ_{23} and δ_{CP}

As stated earlier, the contour plots also give information about the precision of θ_{23} and δ_{CP}. In general the presence of degenerate solutions leads to a worse precision (a larger width of the allowed area) in these parameters. For most values of true δ_{CP} and θ_{23}, there is a negligible difference between the δ_{CP} precision of NOνA$[6+0]$ and NOνA$[3+3]$ around the true point. While there is a qualitative advantage to including both neutrinos and antineutrinos because of their different dependences on δ_{CP}, this advantage is squandered by the lower cross section of antineutrinos. The precision in these parameters can be quantified using the following formulas:

$$CP \text{ precision} = \frac{\delta_{CP}^{\text{Max}} - \delta_{CP}^{\text{Min}}}{360^\circ} \times 100\% \tag{9}$$

$$\theta_{23} \text{ precision} = \frac{\theta_{23}^{\text{Max}} - \theta_{23}^{\text{Min}}}{\theta_{23}^{\text{Max}} + \theta_{23}^{\text{Min}}} \times 100\%. \tag{10}$$

In Table IV, we list the values of the 1σ and 2σ precision of θ_{23} and δ_{CP} using these expressions for the case of NOνA$[3+3]$ + T2K$[8+0]$ + ICAL. The CP precision is seen to be better for $\delta_{CP} = 0^\circ$ as compared to $\delta_{CP} = \pm 90^\circ$ for a given true value of θ_{23}. This is because in the absence of degeneracies the precision simply follows from the probability expression, where $dP_{\mu e}/d\delta_{CP}$ is smallest at 0° [25]. On the other hand, for a given value of δ_{CP}, the CP precision is seen to become worse with increasing θ_{23}. The θ_{23} precision is worse near maximal mixing and improves as one moves away.

IV. CONCLUSION

In the era when the value of θ_{13} was unknown, an eightfold degeneracy of neutrino oscillation parameters was identified, which included the intrinsic θ_{13}, hierarchy-δ_{CP} and octant degeneracies. With the precise measurement of θ_{13}, the intrinsic degeneracy is largely removed, and a four-fold degeneracy out of the original eight—involving wrong-hierarchy and wrong-octant solutions—remains to be solved by the current and upcoming experiments. In this paper, we study these degeneracies in detail and propose that the remaining degeneracies can be studied in the most comprehensive manner by considering the generalized hierarchy-$\theta_{23} - \delta_{CP}$ degeneracy. This degeneracy is continuous for the $P_{\mu e}$ channel. The addition of information on the measurement of θ_{23} by the $P_{\mu\mu}$ channel gives rise to discrete solutions. These are best visualized by contours in the test $(\theta_{23} - \delta_{CP})$ plane drawn for both right and wrong hierarchy for different representative values of true parameters. We show that, depending on whether the wrong-hierarchy and/or wrong-octant solutions occur with right or wrong values of δ_{CP}, there can be a total of eight possibilities. We study these possibilities at the probability level for T2K and NOνA. At this level, the degeneracy is defined as the equality of the probabilities for different values of parameters. However, at the χ^2 contour level, because of the precision of the experiments, one gets finite allowed regions corresponding to degenerate solutions. We define a degenerate solution to be one which is distinct from the true solution at the 1σ level.

Taking only the neutrino run of NOνA as an illustrative example, we identify which of these degenerate solutions actually occur for different representative choices of true parameters. The sample true values that we consider for obtaining the contours are $\theta_{23} = 39^\circ, 42^\circ, 48^\circ$ and 51° and $\delta_{CP} = \pm 90^\circ, 0^\circ$. At the present level of precision, for $\delta_{CP} = \pm 90^\circ$, the right (wrong) δ_{CP} solutions are those which occur in the same (opposite) half-plane as compared to the true solution. Since $\delta_{CP} = 0^\circ$ is common to both half-planes, for this case, the right and wrong δ_{CP} solutions at a particular C.L. are inferred from the nature of the contours. The different degenerate solutions obtained are the (i) WH-WO-Rδ_{CP}, (ii) RH-WO-Wδ_{CP}, (iii) WH-RO-Rδ_{CP}, (iv) RH-RO-Wδ_{CP} and (v) WH-WO-Wδ_{CP} regions. Although the options i–iii have been noticed in the literature earlier, the option iv which exists for the same true θ_{23} but different δ_{CP} has not been discussed extensively. A probability level discussion was done in Ref. [68], where it was called $\theta_{23} - \delta_{CP}$

degeneracy. However, since it can occur for the same hierarchy and same θ_{23}, we call it "intrinsic CP degeneracy." The WH-WO-Wδ_{CP} solutions often appear as part of i, given the CP precision of the current experiments. We identify a few points in the true parameter space where this solution appears as a distinct degenerate solution. Note that for a true value of θ_{23} in the range 48°–51° and δ_{CP} in the lower half-plane ($-180° < \delta_{CP} < 0°$), the NOνA neutrino probability being highest cannot be matched by any other combination, and hence no degenerate solutions appear. In this case, only the neutrino run is better as it gives a better precision. In all other cases that we have studied, 3 years of the neutrino and 3 years of the antineutrino run of NOνA are helpful in removing the wrong-octant solutions i, ii and v to a large extent. This also improves the CP precision since the wrong δ_{CP} solutions occurring with the wrong octant are resolved. Next, we present the results combining NOνA$[3+3]$ with T2K$[8+0]$. It is seen that the synergy between T2K and NOνA helps in removing the WH-RO-Wδ_{CP} solutions for true $\delta_{CP} = 0°$, 90°. For true $\delta_{CP} = -90°$, NOνA itself is sufficient for removing this degeneracy. The precision of both parameters also improves when these two sets of information are compounded together. The remaining degenerate solutions at 2σ can be resolved by adding ICAL data. The latter is seen to play an important role in removing the wrong-hierarchy solution for $\theta_{23} = 48°$. In conclusion, we show that the combination of data from different LBL and atmospheric neutrino experiments can play a crucial role in removing the degeneracies associated with neutrino oscillation parameters, thereby improving the precision of the parameters θ_{23} and δ_{CP}. This also paves the way toward an unambiguous determination of these parameters.

APPENDIX: SYNERGY BETWEEN APPEARANCE AND DISAPPEARANCE CHANNEL AND ROLE OF ANTINEUTRINOS

In this Appendix, we discuss the origin of discrete degenerate regions in the test ($\delta_{CP} - \theta_{23}$) plane from the combination of appearance and disappearance channels for NOνA. We demonstrate the role of antineutrinos in resolving the degeneracies. The reference true point chosen in generating the data is $\delta_{CP} = -90°$ and $\theta_{23} = 39°$. In the upper row of Fig. 6, we plot the sensitivity of NOνA$[6+0]$. The serpentine curves in the top-left panel of Fig. 6 represent the allowed area at 90% C.L. from only the appearance channel. The area inside the vertical curves represents the allowed area from only the disappearance channel at the same C.L. The area between the blue dotted (magenta dotted) curves denotes the region obtained for the right (wrong) hierarchy. For the appearance channel, the allowed region is continuous, and no discrete degenerate solutions appear. This can be understood in the following manner. In the neutrino appearance channel, $\delta_{CP} = -90°$ corresponds to the maximum value in the probability. As one moves away from −90°, the probability decreases and reaches its minimum value at +90°. On the other hand, the probability increases (decreases) as θ_{23} increases (decreases). So if we draw an imaginary horizontal line and an imaginary vertical line at the true point, then the allowed region is expected to come along the diagonal of the rectangle obtained by the intersection of these two imaginary lines and the X, Y axes for $\theta_{23} > 39°$ and $\delta_{CP} \leq +90°$. For $\delta_{CP} > +90°$, the probability starts to increase, so θ_{23} has to fall to keep the probability same. This explains the serpentine nature of the allowed area. The width of the band corresponds to the θ_{23} precision of the experiment. For the disappearance channel, the allowed region is in the vicinity of θ_{23} and $\pi/2 - \theta_{23}$ and parallel to the δ_{CP} axis since the $P_{\mu\mu}$ probability has a very weak dependence on δ_{CP}. However, the combination of the disappearance and appearance channels gives discrete regions in the parameter space due to the excellent θ_{23} precision of the disappearance channel near $\theta_{23} = 39°$ and 51°. This helps to exclude the other wrong values of θ_{23}. This is shown in the top right panel of Fig. 6. Apart from the allowed regions around the true value, one can identify the distinct degenerate solutions corresponding to wrong hierarchy-wrong octant-right δ_{CP} (WH-WO-Rδ_{CP}) and right hierarchy-wrong octant-wrong δ_{CP} (RH-WO-Wδ_{CP}) regions.

To show the exact synergy between the appearance and disappearance channels, in the middle panel of the top row, we plot the χ^2 as a function of θ_{23}(test) for a fixed δ_{CP} value of −90° for the same hierarchy (NH). This figure shows that, though the disappearance channel suffers from the intrinsic octant degeneracy and does not have any octant sensitivity itself ($\chi^2 \sim 0$), when added to the appearance channel, the channel is responsible for that of δ_{CP}.

Next, we discuss the role of antineutrino runs in NOνA. In the bottom row of Fig. 6, we plot the same figures as the top row but for the 3 year neutrino + 3 year antineutrino run. In the bottom left panel, we see that when antineutrino information is added to neutrino data, the allowed region from the appearance channel is significantly reduced. The reason is as follows: as δ_{CP} changes its sign for antineutrinos, the serpentine shape of the allowed region gets flipped with respect to δ_{CP}. This excludes the right hierarchy-wrong octant regions of $\delta_{CP} \in$ UHP (i.e. RH-WO-Wδ_{CP}) and the wrong hierarchy-wrong octant regions of $\delta_{CP} \in$ LHP (i.e. WH-WO-Rδ_{CP}). Thus, after adding the antineutrino data, only the RH-RO-Rδ_{CP} solution remains, as can be seen from the third panel in the bottom row. From the NOνA antineutrino probability figure in the top right panel of Fig. 1, it is seen that the probability of the true point cannot be matched by any points in the NH-HO or IH-HO bands. This means that for this true point, antineutrinos are free from the degeneracies that appear with the wrong octant in neutrinos. Thus, the addition of antineutrino information removes the wrong-octant solutions of NOνA$[6+0]$ that appear in the top right panels of Fig. 6.

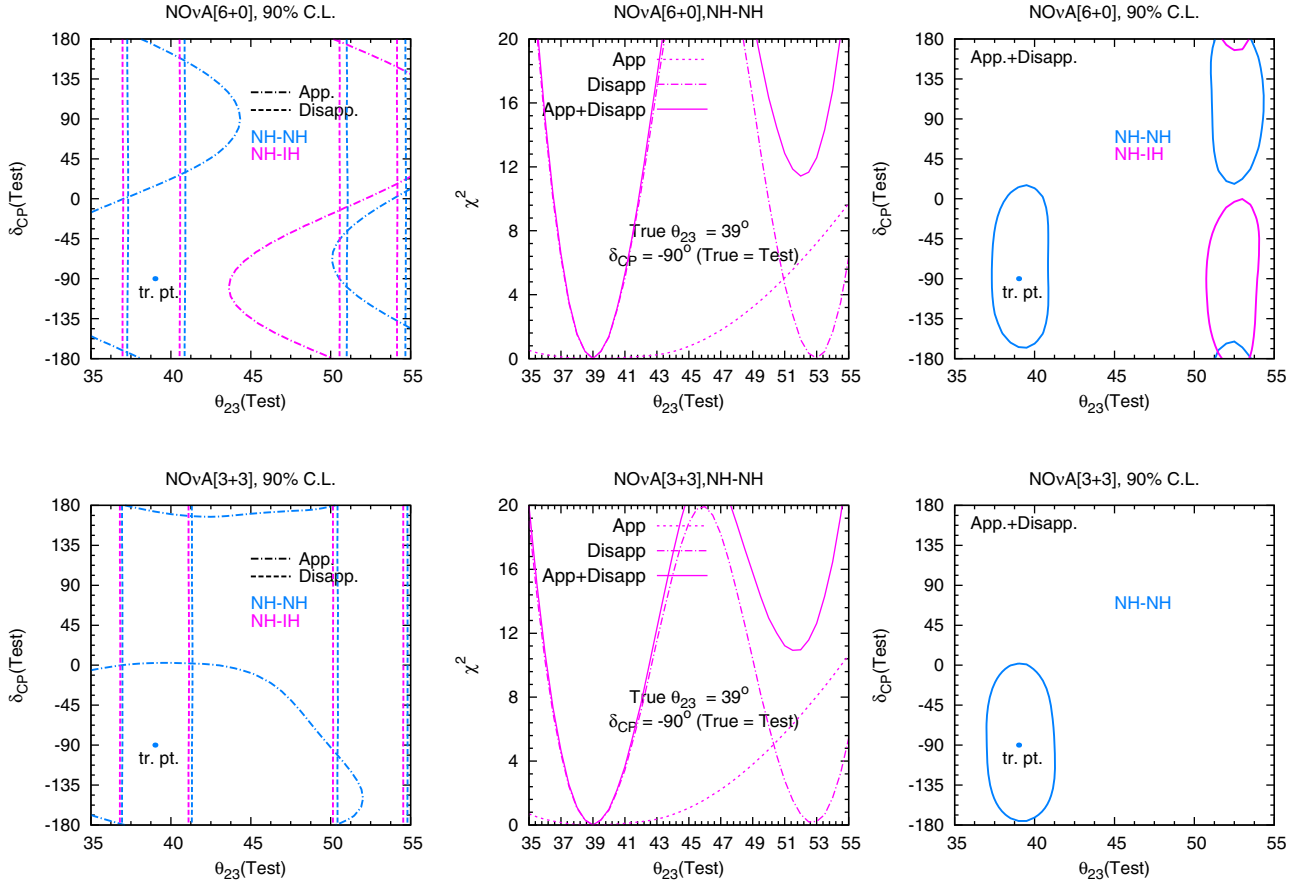

FIG. 6. The plots in the upper row are for NOνA running only in the neutrino mode i.e. NOνA$[6+0]$. Those in the lower row are for NOνA running in equal neutrino and antineutrino mode i.e NOνA$[3+3]$. To generate these plots, we have assumed true $\theta_{23} = 39°$, true $\delta_{CP} = -90°$ and true hierarchy = NH, whereas test parameters are marginalized over the range given in Table II. The plots in the middle panel are generated for a fixed value of the test δ_{CP} $(= -90°)$.

The nature of the disappearance channel contours are seen to remain unaltered, but now the allowed area is slightly broader. This is because of a reduction in the overall statistics due to the smaller cross sections of the antineutrinos. This is also seen in the middle panels where the widths of the χ^2 contours increase.

[1] M. Gonzalez-Garcia, M. Maltoni, and T. Schwetz, J. High Energy Phys. 11 (2014) 052.
[2] F. Capozzi, G. L. Fogli, E. Lisi, A. Marrone, D. Montanino, and A. Palazzo, Phys. Rev. D **89**, 093018 (2014).
[3] D. Forero, M. Tortola, and J. Valle, Phys. Rev. D **90**, 093006 (2014).
[4] V. Barger, D. Marfatia, and K. Whisnant, Phys. Rev. D **65**, 073023 (2002).
[5] J. Burguet-Castell, M. Gavela, J. Gomez-Cadenas, P. Hernandez, and O. Mena, Nucl. Phys. **B646**, 301 (2002).
[6] H. Minakata and H. Nunokawa, J. High Energy Phys. 10 (2001) 001.
[7] G. L. Fogli and E. Lisi, Phys. Rev. D **54**, 3667 (1996).
[8] T. Kajita, H. Minakata, S. Nakayama, and H. Nunokawa, Phys. Rev. D **75**, 013006 (2007).
[9] K. Abe *et al.* (T2K Collaboration), Phys. Rev. Lett. **107**, 041801 (2011).
[10] Y. Abe *et al.* (Double Chooz Collaboration), J. High Energy Phys. 10 (2014) 086.
[11] F. An *et al.* (Daya Bay Collaboration), Nucl. Instrum. Methods Phys. Res., Sect. A **773**, 8 (2015).
[12] J. Ahn *et al.* (RENO Collaboration), Phys. Rev. Lett. **108**, 191802 (2012).
[13] A. Donini, D. Meloni, and P. Migliozzi, Nucl. Phys. **B646**, 321 (2002).
[14] V. Barger, D. Marfatia, and K. Whisnant, Phys. Rev. D **66**, 053007 (2002).

[15] O. Mena, S. Palomares-Ruiz, and S. Pascoli, Phys. Rev. D **73**, 073007 (2006).
[16] M. Narayan and S. U. Sankar, Phys. Rev. D **61**, 013003 (1999).
[17] M. Ishitsuka, T. Kajita, H. Minakata, and H. Nunokawa, Phys. Rev. D **72**, 033003 (2005).
[18] K. Hagiwara, N. Okamura, and K. ichi Senda, Phys. Lett. B **637**, 266 (2006).
[19] V. Barger, D. Marfatia, and K. Whisnant, Phys. Lett. B **560**, 75 (2003).
[20] P. Huber, M. Lindner, and W. Winter, Nucl. Phys. **B654**, 3 (2003).
[21] P. Huber, M. Lindner, T. Schwetz, and W. Winter, Nucl. Phys. **B665**, 487 (2003).
[22] O. Mena and S. J. Parke, Phys. Rev. D **70**, 093011 (2004).
[23] O. Mena, Mod. Phys. Lett. A **20**, 1 (2005).
[24] H. Minakata and H. Sugiyama, Phys. Lett. B **580**, 216 (2004).
[25] S. Prakash, S. K. Raut, and S. U. Sankar, Phys. Rev. D **86**, 033012 (2012).
[26] S. K. Agarwalla, S. Prakash, S. K. Raut, and S. U. Sankar, J. High Energy Phys. 12 (2012) 075.
[27] M. Blennow, P. Coloma, A. Donini, and E. Fernandez-Martinez, J. High Energy Phys. 07 (2013) 159.
[28] K. Hiraide, H. Minakata, T. Nakaya, H. Nunokawa, H. Sugiyama, W. J. C. Teves, and R. Z. Funchal, Phys. Rev. D **73**, 093008 (2006).
[29] H. Minakata, H. Sugiyama, O. Yasuda, K. Inoue, and F. Suekane, Phys. Rev. D **68**, 033017 (2003).
[30] S. Prakash, S. K. Raut, and S. U. Sankar, Phys. Rev. D **86**, 033012 (2012).
[31] A. Chatterjee, P. Ghoshal, S. Goswami, and S. K. Raut, J. High Energy Phys. 06 (2013) 010.
[32] S. K. Agarwalla, S. Prakash, and S. U. Sankar, J. High Energy Phys. 07 (2013) 131.
[33] P. Machado, H. Minakata, H. Nunokawa, and R. Z. Funchal, J. High Energy Phys. 05 (2014) 109.
[34] M. Ghosh, S. Goswami, and S. K. Raut, arXiv:1409.5046.
[35] M. Banuls, G. Barenboim, and J. Bernabeu, Phys. Lett. B **513**, 391 (2001).
[36] J. Bernabeu, S. Palomares-Ruiz, A. Perez, and S. Petcov, Phys. Lett. B **531**, 90 (2002).
[37] J. Bernabeu, S. Palomares-Ruiz, and S. Petcov, Nucl. Phys. **B669**, 255 (2003).
[38] R. Gandhi, P. Ghoshal, S. Goswami, P. Mehta, and S. U. Sankar, Phys. Rev. D **73**, 053001 (2006).
[39] S. Palomares-Ruiz and S. Petcov, Nucl. Phys. **B712**, 392 (2005).
[40] D. Indumathi and M. Murthy, Phys. Rev. D **71**, 013001 (2005).
[41] S. Petcov and T. Schwetz, Nucl. Phys. **B740**, 1 (2006).
[42] R. Gandhi, P. Ghoshal, S. Goswami, P. Mehta, S. U. Sankar, and S. Shalgar, Phys. Rev. D **76**, 073012 (2007).
[43] A. Samanta, Phys. Lett. B **673**, 37 (2009).
[44] M. M. Devi, T. Thakore, S. K. Agarwalla, and A. Dighe, J. High Energy Phys. 10 (2014) 189.
[45] A. Ghosh, T. Thakore, and S. Choubey, J. High Energy Phys. 04 (2013) 009.
[46] A. Ghosh and S. Choubey, J. High Energy Phys. 10 (2013) 174.
[47] R. Gandhi, P. Ghoshal, S. Goswami, and S. U. Sankar, Phys. Rev. D **78**, 073001 (2008).
[48] V. Barger, R. Gandhi, P. Ghoshal, S. Goswami, D. Marfatia, S. Prakash, S. K. Raut, and S. U. Sankar, Phys. Rev. Lett. **109**, 091801 (2012).
[49] M. Gonzalez-Garcia, M. Maltoni, and A. Y. Smirnov, Phys. Rev. D **70**, 093005 (2004).
[50] S. Choubey and P. Roy, Phys. Rev. D **73**, 013006 (2006).
[51] P. Huber, M. Maltoni, and T. Schwetz, Phys. Rev. D **71**, 053006 (2005).
[52] M. Blennow and T. Schwetz, J. High Energy Phys. 08 (2012) 058.
[53] S. Choubey and A. Ghosh, J. High Energy Phys. 11 (2013) 166.
[54] P. Coloma, H. Minakata, and S. J. Parke, Phys. Rev. D **90**, 093003 (2014).
[55] P. Huber, M. Lindner, and W. Winter, Comput. Phys. Commun. **167**, 195 (2005).
[56] P. Huber, J. Kopp, M. Lindner, M. Rolinec, and W. Winter, Comput. Phys. Commun. **177**, 432 (2007).
[57] M. D. Messier, Ph.D. Thesis, Boston University Graduate School of Arts and Science, 1999.
[58] E. Paschos and J. Yu, Phys. Rev. D **65**, 033002 (2002).
[59] Y. Itow *et al.* (T2K Collaboration), arXiv:hep-ex/0106019.
[60] Http://t2k-experiment.org/2015/05/t2k-releases-its-first-measurement-of-muon-antineutrino-disappearance/.
[61] R. Patterson (NOνA Collaboration), *Neutrino 2012 Conference*, Kyoto, Japan, 2012 (unpublished).
[62] A. Chatterjee, K. K. Meghna, R. Kanishka, T. Thakore, V. Bhatnagar, R. Gandhi, D. Indumathi, N. K. Mondal, and N. Sinha, J. Instrum. **9**, P07001 (2014).
[63] M. C. Gonzalez-Garcia and M. Maltoni, Phys. Rev. D **70**, 033010 (2004).
[64] G. Fogli, E. Lisi, A. Marrone, D. Montanino, and A. Palazzo, Phys. Rev. D **66**, 053010 (2002).
[65] E. K. Akhmedov, R. Johansson, M. Lindner, T. Ohlsson, and T. Schwetz, J. High Energy Phys. 04 (2004) 078.
[66] A. Cervera, A. Donini, M. B. Gavela, J. J. G. Cádenas, P. Hernández, O. Mena, and S. Rigolin, Nucl. Phys. **B579**, 17 (2000).
[67] M. Freund, Phys. Rev. D **64**, 053003 (2001).
[68] H. Minakata and S. J. Parke, Phys. Rev. D **87**, 113005 (2013).
[69] M. Ghosh, P. Ghoshal, S. Goswami, and S. K. Raut, Phys. Rev. D **89**, 011301 (2014).
[70] M. Ghosh, P. Ghoshal, S. Goswami, and S. K. Raut, Nucl. Phys. **B884**, 274 (2014).
[71] S. Razzaque and A. Yu. Smirnov, J. High Energy Phys. 05 (2015) 139.